A mathematical model to study the impact of intra-tumour heterogeneity on anti-tumour CD8 + T cell immune response

Emma Leschiera, Tommaso Lorenzi, Shensi Shen, Luis Almeida, Chloe Audebert

A mathematical model to study the impact of intra-tumour heterogeneity on anti-tumour CD8$^+$ T cell immune response

Emma Leschiera*[1], Tommaso Lorenzi[2], Shensi Shen[3], Luis Almeida[1], and Chloe Audebert[5,6]

[1]*Sorbonne Université, CNRS, Université de Paris, Inria, Laboratoire Jacques-Louis Lions UMR 7598, 75005 Paris, France.*
[2]*Department of Mathematical Sciences "G. L. Lagrange", Dipartimento di Eccellenza 2018-2022, Politecnico di Torino, 10129 Torino, Italy.*
[3]*Institute of Thoracic Oncology, West China Hospital, Sichuan University, Chengdu, China.*
[4]*Sorbonne Université, CNRS, Université de Paris, Laboratoire Jacques-Louis Lions UMR 7598, 75005 Paris, France.*
[5]*Sorbonne Université, CNRS, Institut de biologie Paris-Seine (IBPS), Laboratoire de Biologie Computationnelle et Quantitative UMR 7238, 75005 Paris, France.*

Abstract

The number of sub-populations of tumour cells constituting a tumour and the immunogenicity of tumour cells are two major components of intra-tumour heterogeneity (ITH), and play a key role in the immune response against solid tumours. Mathematical models make it possible to separate these two components of ITH and investigate their influence on anti-tumour immunity in a controlled manner. Here, we present a spatially explicit stochastic individual-based model of the interaction dynamics between tumour cells and CD8$^+$ T cells. We use this model to investigate how ITH may affect the anti-tumour immune response. In our model, ITH can vary both with the number of expressed antigens (*i.e.* the number of sub-populations of tumour cells) and with the level of antigen presentation (*i.e.* the immunogenicity of the cells). Computational simulations of our model indicate that both sources of ITH affect the outcome of anti-tumour immune response. First, the number of sub-populations of tumour cells negatively correlates with the ability of the CD8$^+$ T cells to produce an efficient anti-tumoural response. Second, the fraction of non-immunogenic cells within a tumour can significantly reduce the effectiveness of the immune response. These results qualitatively reproduce a broad range of scenarios of successful and unsuccessful immune surveillance reported in experimental studies. Ultimately, our model may provide a framework to help biologists and clinicians to better understand the prognostic outcomes of immunotherapy.

Keywords: Individual-based models; Numerical simulations; Tumour-Immune cell interactions; Intra-tumour heterogeneity; Antigen presentation

*Corresponding author
Email addresses: leschiera@ljll.math.upmc.fr (Emma Leschiera), tommaso.lorenzi@polito.it (Tommaso Lorenzi), shenshensi@wchscu.cn (Shensi Shen), almeida@ljll.math.upmc.fr (Luis Almeida), chloe.audebert@sorbonne-universite.fr (Chloe Audebert).
E.L. has received funding from the European Research Council (ERC) under the European Union's Horizon2020 research and innovation programme (grant agreement No 740623).
T.L. gratefully acknowledges support of the MIUR grant "Dipartimenti di Eccellenza 2018-2022".

1 Introduction

Recent technological advances have allowed for the design of immunotherapy which, in contrast to conventional anti-cancer therapies, targets tumour-immune cell interactions with the aim of re-boosting the effectiveness of the anti-tumoural immune responses. Although immunotherapy has revolutionized anti-tumour treatment, its efficacy remains limited in most clinical settings [3, 9, 10, 27, 68, 74].
Immune cells, specifically $CD8^+$ cytotoxic T cells, are capable of detecting and eliminating tumour cells by recognising cancer-associated antigens expressed by tumour cells. The effectiveness of the immune response depends on the level of presentation of such antigens by the major histocompatibility complex 1 (MHC-I) [20, 60]. In particular, $CD8^+$ T cells express a unique repertoire of T cell receptors (TCRs) [65] and, once activated, they migrate via chemotaxis in response to concentration gradients of chemical signals toward the tumour cells expressing the matching antigens [62]. The influx and movement of $CD8^+$ T cells are dictated by the spatial distribution of tumour antigens and by the level of chemokines in the tumour micro-environment [10]. Upon intratumoural infiltration, $CD8^+$ T cells can trigger tumour cell death by direct interaction with tumour cells, releasing cytotoxic factors (*i.e.* granzime B, interferon gamma) [44].

Oncogenic mutation-driven cancers harbor neoantigens that can be recognized by $CD8^+$ T cell receptors [35]. A high mutational burden and neoantigen load in tumours have been associated with an enhanced response to immunotherapy [15, 30, 37, 69, 70, 76]. However, it has recently been reported that many of these neoantigens arise from sub-clonal branching mutations and could potentially increase intratumour heterogeneity (ITH) [57, 59, 67]. In particular, in these tumours, the antigen landscape is composed of clonal antigens, presented by all tumour cells, and sub-clonal antigens, presented only by sub-populations of tumour cells. Moreover, such sub-clonal antigens may be associated with decreased level of antigen presentation by the MHC-I, leading to a weaker antigen-specific $CD8^+$ T cell response [29]. In contrast, more homogeneous tumours express few clonal antigens in all tumour cells and appear to have a better response to immunotherapy across a wide range of tumour types [26, 59]. Furthermore, $CD8^+$ T cells activated against clonal antigens are more commonly found at the tumour site than $CD8^+$ T cells reactive to sub-clonal antigens [59]. These findings point to ITH as a highly relevant determinant of tumour immune surveillance that deserves further consideration.

Mathematical models are useful tools for simulating and investigating biological systems, and have been increasingly used to investigate the role of tumour antigens and the effect of ITH on the anti-tumour immune response. Tumour heterogeneity and the role of tumour antigens have been studied using differential equation models [1, 6, 8, 50] and cellular-automaton (CA) models [11, 31]. A number of mathematical models have also been developed to investigate the dynamics of tumour development in the presence of adaptive immune response. Usually, these models are formulated as either ordinary differential equations [21, 45, 47, 51] or integro-differential equations [23, 46, 49]. Most of these models rely on the assumption that cells are well-mixed and, as such, do not take into account spatial dynamics of immune cells and tumour cells. Spatial and temporal dynamics of tumour-immune competition have been studied through partial differential equation (PDE) models [7, 55, 56]. However, differential equation models are defined on the basis of population-level phenomenological assumptions, which may limit the level of biological detail that can be included in the model. By using computational models, such as CA and individual-based models (IBMs), a more direct and precise mathematical representation of biological phenomena can be achieved. These models can be posed on a spatial domain (*e.g.* a grid), where cells interact locally with each other according

to a defined set of probabilistic rules, and can collectively generate global emergent behaviours of tumour-immune cells interaction. A number of IBMs [19, 41, 52] and hybrid PDE-CA models [22, 43, 54] have also been used to study the interaction dynamics between tumour and immune cells. These models take into account different aspects of the anti-tumoural immune response (*e.g.* expression of immunosuppressive factors, movement of immune cells) and clarify the conditions for the emergence of a range of situations of successful and failed immune response. However, they do not take into account the effects of antigen presentation and ITH on immune surveillance.

In light of these considerations, we present a spatial stochastic individual-based model of tumour-immune interaction dynamics that can be used to explore the effect of ITH on immune surveillance. The originality of this model lies in the characterization of antigen presentation levels by tumour cells, which drive the influx of $CD8^+$ T cells in the tumour micro-environment and their movement toward tumour cells. In our model, the effectiveness of the anti-tumour immune response directly correlates with the level of presentation of tumour antigens. In addition, the model takes into account biological phenomena that are driven by stochastic aspects of the interaction dynamics between tumour cells and $CD8^+$ T cells. The effect of ITH on immune surveillance is investigated at two different levels through computational simulations of this model. First, we explore the outcomes of the immune response considering different number of sub-populations of tumour cells constituting the tumour. Then, we asses the efficiency of the immune response by varying the immunogenicity of tumour cells. We study the impact of these two characteristics on tumour progression independently and together, assessing their influence on anti-tumour immunity in a controlled manner.

The paper is organised as follows. In Section 2, we present the individual-based model and the mathematical description of each biological process included in the model. Section 3 summarises the set-up of computational simulations. Full details of model implementation and model parametrisation are provided in A and B, respectively. In Section 4 we present the main computational results and we discuss them in view of previous biological works. Finally, Section 5 concludes the paper and provides a brief overview of possible research perspectives.

2 Model and methods

We consider two cell types in our model: tumour cells, characterized by an antigen profile and a level of antigen presentation, and antigen-specific $CD8^+$ T cells. To describe the interactions occurring between the two cell types we use an on-lattice individual-based model posed on a 2D spatial domain partitioned into square elements of side Δx. In our model, this domain biologically represents the tumour micro-environment. At each time step of length Δt, the states of the cells are updated according to the probabilistic and deterministic rules described below.
In the remainder of this section, we first present the modelling framework in a general setting, along with the underlying biological hypotheses and assumptions. Then, we detail how each biological mechanism is mathematically described. A detailed description of the computational implementation of the model, which relies on a Cellular Potts approach, can be found in A.

2.1 Modelling framework

To include different level of immunogenicity in the tumour, two different subtypes of tumour cells are considered: immunogenic cells and non-immunogenic cells. On the one hand, we define immunogenic cells as cells expressing one or more clonal antigens, considered as immunodominant, and presented at a normal level by the MHC-I. On the other hand, we assume that

non-immunogenic cells have experienced, through mutations, a deterioration of their level of antigen presentation, and have acquired new antigens, presented only by a subset of tumour cells, to which we refer as sub-clonal antigens [59]. Therefore, we define non-immunogenic cells as cells expressing clonal and sub-clonal antigens, both presented at a low level by the MHC-I.
The system is initially composed of tumour cells only, which grow and proliferate through mitosis. Tumour cells secrete different chemoattractants that trigger the influx of specific $CD8^+$ T cells into the domain. When they arrive in the domain, $CD8^+$ T cells move via chemotaxis toward tumour cells expressing the matching antigens and, upon contact, try to eliminate them.
The modelling strategies used to reproduce these dynamics are described in detail in the following subsections, and are also schematically illustrated with an example in Figure 1 and Figure 2.

2.1.1 Dynamics of tumour cells

Antigen expression We let $N_T(t)$ denote the number of tumour cells in the system at time $t = h\Delta t$, with $h \in \mathbb{N}_0$, and we label each cell by an index $n = 1, \dots, N_T(t)$. We let each tumour cell express one or more antigens, and we characterize the antigen profile of the tumour by means of a vector

$$A = (a_1, \dots, a_f), \quad a_1, \dots, a_f \in \mathbb{N}, \tag{2.1}$$

where a_i denotes an antigen and f is the total number of antigens expressed by the tumour [see Figure 1(a)]. Using phylogenetic tree representations [see Figure 1(b)-(c)], we define each antigen $a_i \in A$, $i = 1, \dots, f$, of the tumour as clonal if it belongs to the trunk of the phylogenetic tree, or sub-clonal if it belongs to one of the branches of the phylogenetic tree. We let A_C and A_{SC} denote the sets of clonal and the sub-clonal antigens, whereby:

$$A_C, A_{SC} \subset A, \quad A_C \cup A_{SC} = A \quad \text{and} \quad A_C \cap A_{SC} = \emptyset. \tag{2.2}$$

Then, based on the phylogenetic tree representation, we divide the tumour in f different subpopulations of tumour cells labelled by the last antigen $a_i \in A$ acquired [see Figure 1(d)]. In each sub-population, cells express the same antigens. Moreover, if $a_i \in A_C$, cells in the subpopulation labelled by the antigen a_i express only clonal antigens, whereas if $a_i \in A_{SC}$, cells in the sub-population labelled by the antigen a_i express both clonal and sub-clonal antigens. Therefore, we define cells in sub-populations labelled by a clonal antigen $a_i \in A_C$ as immunogenic cells, whereas cells in sub-populations labelled by a sub-clonal antigen $a_i \in A_{SC}$ are defined as non-immunogenic cells.

Antigen presentation by MHC-I We incorporate antigen presentation into our model by letting each tumour cell present its antigens at a certain level. There can be high variability in each antigen's presentation between patients with the same type of tumour and even within tumour cell samples from the same patient [3, 59]. Therefore, for the n^{th} tumour cell, we characterize the level of presentation of each one of its antigens $a_i \in A$ by the normalized variable

$$l^n_{a_i} \in [0, 1] \tag{2.3}$$

whereby the value $l^n_{a_i} = 0$ corresponds to a tumour cell that lost the expression of the antigen a_i, while $l^n_{a_i} = 1$ corresponds to a tumour cell presenting the antigen a_i at the highest level.
To capture the idea that immunogenic cells present their antigens at a higher level than non-immunogenic cells, we introduce the discrete sets

$$L_I = \{\mathrm{m}_I, \dots, \mathrm{M}_I\} \subset [0, 1] \text{ and } L_{NI} = \{\mathrm{m}_{NI}, \dots, \mathrm{M}_{NI}\} \subset [0, 1], \text{ with } \mathrm{M}_{NI} < \mathrm{M}_I. \tag{2.4}$$

They characterize the range of different values that can be taken by the variable $l^n_{a_i}$ [see Figure 1(d)]. In particular, if the n^{th} tumour cell is an immunogenic cell, it presents each antigen a_i

at a normal level $l^n_{a_i} \in L_I$, whereas if the n^{th} tumour cell is a non-immunogenic cell, all of its antigens a_i are presented at a low level $l^n_{a_i} \in L_{NI}$.

Tumour cell growth and division At each time-step, we let tumour cells grow at a random rate drawn from a uniform distribution; the parameters of the bounds of the uniform distribution are chosen to match the mean duration of a tumour cell cycle length. Mitosis occurs when a tumour cell grows to a critical size and then divides along a randomly orientated axis. Upon division at the time t, the n^{th} tumour cell is replaced by two cells [see Figure 1(e)], one labelled by the parent index n and the other one labelled by the index $N_T(t) + 1$. Note that the total number of tumour cells $N_T(t)$ is updated as soon as a cell divides, and before looping on the next proliferating cell. The daughter cell will inherit most of the properties of the parent cell, including the antigens expressed by the parent cell, so the fact that the cell is immunogenic or not [see Figure 1(e)]. For each antigen a_i expressed by the daughter cell, a random level of antigen presentation $l^{N_T(t)+1}_{a_i}$ will be chosen. Another property not inherited by the daughter cell is the intrinsic lifespan of the cell, which is randomly drawn from a uniform distribution.

Tumour cell death If a tumour cell exhausts its lifespan (which is drawn when the cell is created), it dies (*i.e.* it undergoes apoptosis) at the end of the time-step and it is removed from the domain. A tumour cell can also die due to intra-tumour competition, with a rate proportional to the total number of tumour cells, or because of the cytotoxic action of $CD8^+$ T cells. More details about tumour cell death due to the cytotoxic action of $CD8^+$ T cells will be given in Section 2.1.2.

Secretion of chemoattractants We let tumour cells at the border of the tumour (the region where cytokines and immune cells are more abundant [10]) secrete different chemoattractants for each expressed antigen $a_i \in A$. The secretion of a chemoattractant by a tumour cell expressing antigen a_i is proportional to the level of presentation of such antigen a_i. Therefore, we model the chemoattractant secretion rate $s^n_{a_i}$ by the n^{th} tumour cell expressing antigen a_i using the following definition:

$$s^n_{a_i} := C_1\, l^n_{a_i}, \tag{2.5}$$

where $C_1 \in \mathbb{R}^+$ is a scaling factor of units $\frac{[mol]}{[time]\,[space]}$, where $[mol]$, $[time]$ and $[space]$ denote respectively the number of chemoattractant molecules and the units of time and of the size of a grid site, and $l^n_{a_i}$ is the level of presentation of antigen a_i by the n^{th} tumour cell.
The total amount of chemoattractant secreted by tumour cells expressing antigen a_i induces the arrival of $CD8^+$ T cells specific to antigen a_i into the domain. More details about the mathematical modelling of the different chemoattractants will be discussed in Section 2.1.3.

2.1.2 Dynamics of $CD8^+$ T cells

Influx of $CD8^+$ T cells Following Gong et al. [32], to model the tumour vessels that allow the arrival of $CD8^+$ T cells in the tumour micro-environment, we generate a set of points in the domain. In order not to rely on a detailed angioarchitecture, we generate 5 entry points, equidistant from each other and from the centre of the domain. At each time step, a $CD8^+$ T cell specific to antigen $a_i \in A$ can be supplied to the domain from one of the 5 entry points, provided that the entry point is not occupied by other cells. The probability $0 < p(t) \leq 1$ of influx of a $CD8^+$ T cell specific to antigen a_i into the domain is proportional to the total amount $S^{tot}_{a_i}(t)$ of chemoattractant associated to antigen a_i secreted at time t. Therefore, we define $p(t)$ as

$$p(t) := C_2\, S^{tot}_{a_i}(t),$$

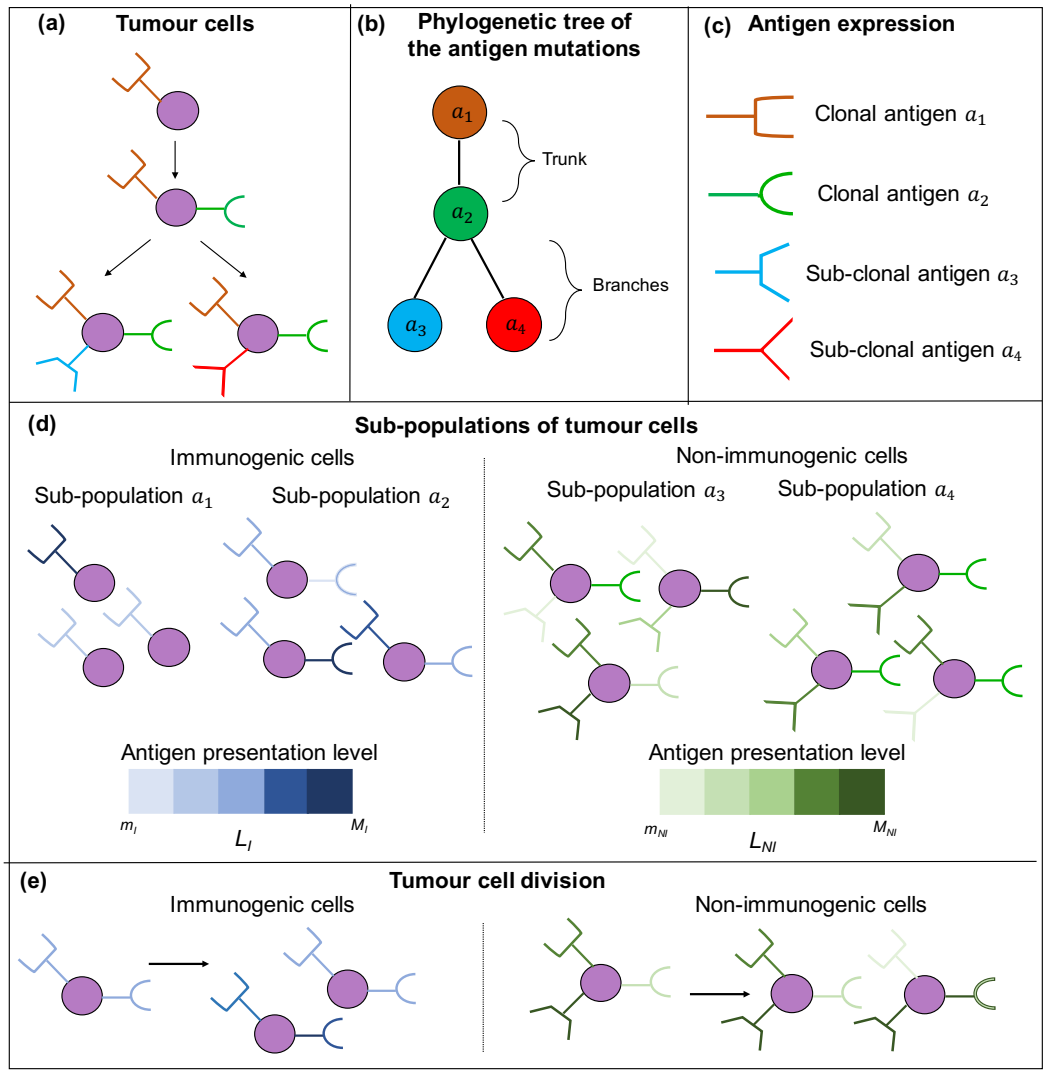

Figure 1: **Schematic representation of the modelling assumptions for tumour cells. (a)** Purple circles represent tumour cells. In this example, the antigen profile of the tumour is characterized by 4 different antigens, each one represented by a specific color and shape. **(b)** Phylogenetic tree illustrating the mutations leading to the different antigens expressed by tumour cells. The clonal and sub-clonal antigens are represented as the phylogenetic tree trunk and branches, respectively. **(c)** In this example, 4 antigens are expressed by the tumour, each one characterized by a different color and shape. Based on the phylogenetic tree **(b)**, we denote a_1 and a_2 as clonal antigens, whereas a_3 and a_4 are denoted as sub-clonal antigens. **(d)** The tumour is divided in 4 sub-populations of tumour cells, labelled by the last antigen acquired by each cell. Here, the color of each antigen represents its level of antigen presentation. Cells in the sub-populations labelled by the antigens a_1 and a_2 express only clonal antigens and are defined as immunogenic cells. They present their antigens at a normal level, with values chosen from the discrete set $L_I = \{\mathrm{m}_I, \ldots, \mathrm{M}_I\}$. Cells in the sub-populations labelled by the antigens a_3 and a_4 express clonal and sub-clonal antigens and are defined as non-immunogenic cells. They present all their antigens at a low level, with values chosen from the discrete set $L_{NI} = \{\mathrm{m}_{NI}, \ldots, \mathrm{M}_{NI}\}$. **(e)** A tumour cell divides when it reaches a certain target volume. An immunogenic (respectively non-immunogenic) cell divide in two immunogenic (respectively non-immunogenic) cells. The daughter cell has the same antigens of the parent cell, but with a new random level of antigen presentation.

with $C_2 \in \mathbb{R}^+$ a scaling factor of units $\frac{[time]}{[mol]}$.
Since the secretion of chemoattractants by tumour cells is proportional to the level of antigen presentation (see Eq. (2.5)), the total amount of chemoattractants secreted by non-immunogenic cells is lower than the total amount of chemoattractants secreted by immunogenic cells. Therefore, the influx of CD8$^+$ T cells targeted to sub-clonal antigens, which are expressed only by non-immunogenic cells, is lower than the influx of CD8$^+$ T cells targeted to clonal antigens.

TCR expression and T cell death We denote by $N_C(t)$ the number of CD8$^+$ T cells in the system at time t, and we label each of them by an index $m = 1, ..., N_C(t)$. Every CD8$^+$ T cell has a unique TCR [see Figure 2(a)], and we suppose that each TCR is specific to a unique tumour antigen [see Figure 2(b)]. When the m^{th} CD8$^+$ T cell with a TCR targeted against antigen $a_i \in A$ arrives into the domain it undergoes chemotactic movement toward tumour cells expressing the matching antigen a_i.
As CD8$^+$ T cell division occurs mostly in the lymph nodes [24], we omit the effects of CD8$^+$ T cell proliferation in the tumour micro-environment. A CD8$^+$ T cell undergoes apoptosis when it reaches the end of its intrinsic lifespan, which is drawn from a uniform distribution upon its arrival in the domain.

Elimination of tumour cells by CD8$^+$ T cells Upon contact, CD8$^+$ T cells can interact only with tumour cells expressing the matching antigen [see Figure 2(c)], and can induce their death, on the condition that the matching antigen is presented at a sufficiently high level. If a CD8$^+$ T cell is in contact with more than one tumour cell expressing the matching antigen, it will try to eliminate the one presenting the antigen at the highest level. In particular, when the m^{th} CD8$^+$ T cell interacts with the n^{th} tumour cell expressing the matching antigen a_i, we let the tumour cell be removed from the system, provided that

$$\mu \, l^n_{a_i} > (1 - r). \tag{2.6}$$

Here μ is a random variable drawn from the standard uniform distribution, $l^n_{a_i}$ is the level of presentation of antigen a_i by the n^{th} tumour cell and $0 < r \leq 1$ is the intrinsic TCR-recognition probability, which we suppose to be equal for every CD8$^+$ T cell. If the tumour cell satisfies the conditions to be eliminated, it undergoes apoptosis. The parameter r determines the range of tumour cells the CD8$^+$ T cell population can interact with: large values of r represent a CD8$^+$ T cell population able to eliminate tumour cells presenting their antigens at a low level, whereas low values of r model the scenario where the CD8$^+$ T cells can only eliminate tumour cells presenting their antigens at a high level.
Tumour cell elimination by CD8$^+$ T cells takes approximately 6 hours to be completed *in vitro* [14] and *in vivo* [12]. Accordingly, we require that an elimination event keeps a CD8$^+$ T cell engaged for 6 hours and only after this time the CD8$^+$ T cell can eliminate again [41].

2.1.3 Chemoattractant field

As mentioned earlier, we let the n^{th} tumour cell at the border of the tumour secrete a different chemoattractant for each antigen a_i that it expresses. Denoting by c_{a_i} the concentration of the chemoattractant secreted by tumour cells expressing antigen a_i, we let the dynamic of c_{a_i} be described by the following reaction-diffusion equation:

$$\frac{\partial c_{a_i}}{\partial t} = D\Delta c_{a_i} - \gamma c_{a_i} + \sum_{n \in N_T(t)} s^n_{a_i}, \quad a_i \in A. \tag{2.7}$$

In Eq. (2.7), D is the diffusion constant and γ is the rate of natural decay; these two parameters are assumed to have the same value for each chemoattractant. On the other hand, we recall

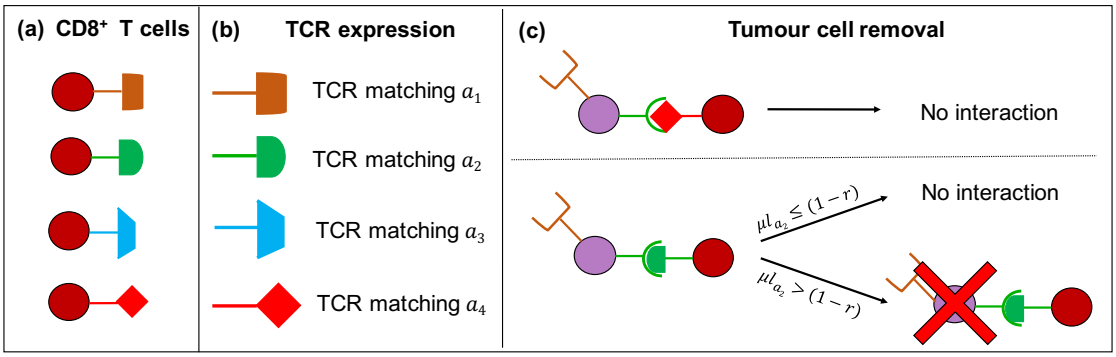

Figure 2: **Schematic representation of the modelling assumptions for CD8$^+$ T cells and their interaction with tumour cells. (a)** Red circles represent CD8$^+$ T cells, which express a unique TCR. **(b)** TCR are represented with different shapes and colors. Each TCR is able to recognize a particular tumour antigen. In the model, the number of TCRs is equal to the number of expressed tumour antigens. **(c)** Purple circles represent tumour cells. CD8$^+$ T cells can eliminate tumour cells, upon contact, under certain conditions. A tumour cell is eliminated if it presents the antigen matching the CD8$^+$ T cell receptor at a sufficiently high level. In this example, a tumour cell expressing antigen a_1 and a_2 cannot be eliminated by a CD8$^+$ T cell with TCR matching antigen a_4. On the other hand, the same tumour cell may be eliminated by a CD8$^+$ T cell expressing the TCR matching antigen a_2, under a condition on the level l_{a_2} of presentation of such antigen a_2. The parameter r is the intrinsic TCR-recognition probability and μ is a random variable drawn from a standard uniform distribution.

that the secretion rate $s^n_{a_i}$ is specific to the n^{th} tumour cell, because it is proportional to the level of presentation of antigen a_i by the tumour cell (see Eq. (2.5)).
We add to Eq. (2.7) zero-flux boundary conditions and an initial concentration c_a^{init} which is set to be zero everywhere in the domain but at the border of the tumour.

3 Numerical simulations

3.1 Set-up of simulations

For numerical simulations of our individual-based model, we use a Cellular Potts approach on a 2D spatial grid with a total of 400×400 lattice sites. Simulations were developed and run using the software CompuCell3D [39] on a standard workstation (Intel i7 Processor, 4 cores, 16 GB RAM, macOS 11.2.2), with one time-step chosen to be $\Delta t = 1$ min. The computational implementation of Cellular Potts models is described in A, while full details of the model parametrisation are provided in B. Files to run a simulation example with Compucell3D software [39] are available at: https://plmlab.math.cnrs.fr/audebert/cc3dmodeltumourcd8.
At the initial time point of the simulation, a certain number of tumour cells are already present in the domain, while CD8$^+$ T cells arrive only when the simulation starts. At the beginning of simulations there is a total of 400 tumour cells, tightly packed in a circular configuration positioned at the centre of the domain, reproducing the geometry of a solid tumour.
All quantities we report in Section 4 are obtained by averaging over the results of 10 simulations. Unless otherwise explicitly stated, we carry out numerical simulations for 28800 time-steps, corresponding to 20 days.

3.2 Initial composition of the tumour

To explore the effects of ITH on immune response, we consider different initial antigenic compositions of the tumour, corresponding to different degrees of ITH. In particular, we dissect out

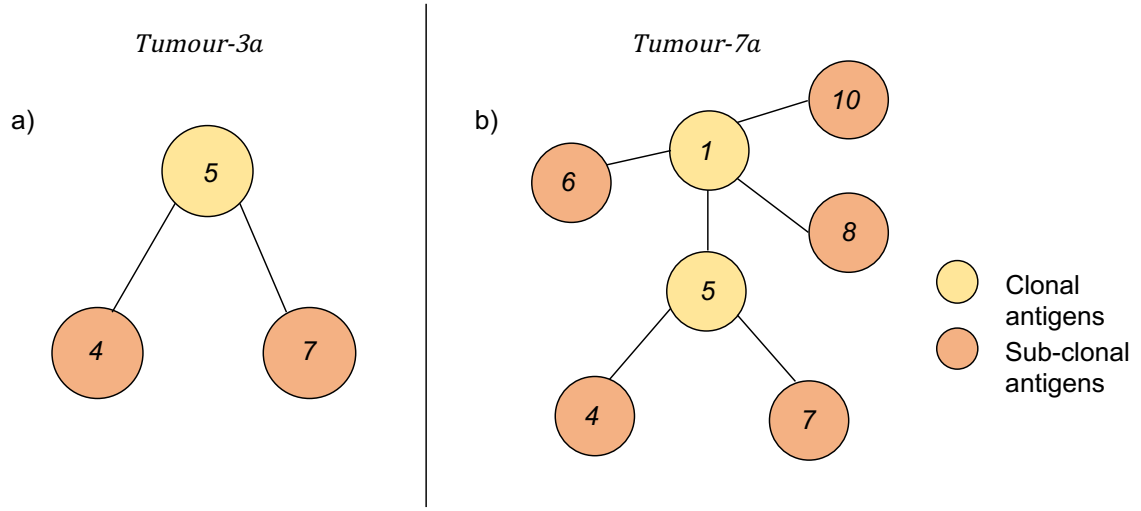

Figure 3: **Phylogenetic tree representations of the antigens considered for the two tumours. (a)** *Tumour-3a* expresses three antigens. Antigen 5 is the only clonal antigen (in yellow) and antigens 4 and 7 are two sub-clonal antigens (in orange). As a results, *tumour-3a* is composed of 3 sub-populations of tumour cells. **(b)** *Tumour-7a* expresses seven antigens. Antigens 1 and 5 are clonal antigens (in yellow) and antigens 4, 6, 7, 8 and 10 are sub-clonal antigens (in orange). Hence, *tumour-7a* is composed of 7 sub-populations of tumour cells. The phylogenetic tree representations of the two tumours are inspired by Wolf et al. [78].

two characteristics of ITH: the number of sub-populations of tumour cells constituting a tumour and the fraction of immunogenic and non-immunogenic cells within it. With our model, we wish to investigate the effect of these two sources of ITH on tumour aggressiveness independently and together, evaluating their influence on anti-tumour immunity in a controlled manner. To this end, first we generate two tumours with different number of sub-populations of tumour cells. For simplicity, we denote the first tumour as *tumour-3a* and the second one as *tumour-7a*. The antigenic composition of the two tumours and their corresponding phylogenetic tree representation are inspired by Wolf et al. [78]. More details about the two tumours are given in the next paragraphs. Next, for each tumour we consider different initial fractions of immunogenic and non-immunogenic cells. When different sub-populations of immunogenic (or non-immunogenic) cells are considered, the total fraction of immunogenic (or non-immunogenic) cells is equally distributed in each sub-population. This enables us to decouple antigen heterogeneity and antigen immunogenicity, and study their influence on tumour aggressiveness in a causal, systematic manner.

Tumour-3a The first tumour we consider expresses three different antigens, one of which is clonal and the other two are sub-clonal (see Figure 3(a)). With the notation introduced in Section 2.1.1, we denote respectively by

$$A = \{4, 5, 7\}, \quad A_C = \{5\} \quad \text{and} \quad A_{SC} = \{4, 7\} \tag{3.1}$$

the antigen profile of the tumour, the clonal antigens and the sub-clonal antigens.
Based on the phylogenetic tree representation of Figure 3(a), we divide *tumour-3a* in 3 sub-populations of tumour cells labelled by the last antigen acquired by each cell. Cells in the sub-population labelled by antigen 5 carry only this antigen, while cells in sub-populations labelled by antigens 4 and 7 express, respectively, antigens 5 and 4 or antigens 5 and 7.
As cells in the sub-population labelled by antigen 5 are immunogenic, their level of antigen presentation by the MHC-I is assumed to be normal and randomly chosen from the discrete set

L_I, which is defined as

$$L_I = \left\{ \frac{1}{6}, \frac{2}{6}, \frac{3}{6}, \frac{4}{6}, \frac{5}{6}, 1 \right\}. \tag{3.2}$$

On the other hand, as cells in sub-populations labelled by antigens 4 and 7 are non-immunogenic, their level of antigen presentation by the MHC-I is deteriorated and, therefore, randomly chosen from the discrete set L_{NI}, which is defined as

$$L_{NI} = \left\{ \frac{5}{100}, \frac{10}{100}, \frac{15}{100}, \frac{20}{100}, \frac{25}{100}, \frac{30}{100} \right\}. \tag{3.3}$$

Tumour-7a The second tumour expresses seven different antigens, two of which are clonal and five are sub-clonal (see Figure 3(b)). We denote respectively by

$$A = \{1, 4, 5, 6, 7, 8, 10\}, \quad A_C = \{1, 5\} \quad \text{and} \quad A_{SC} = \{4, 6, 7, 8, 10\} \tag{3.4}$$

the antigen profile of the tumour, the clonal antigens and the sub-clonal antigens.
Based on the phylogenetic tree representation of Figure 3(b), we divide *tumour-7a* in 7 sub-populations of tumour cells. Cells in sub-populations labelled by antigens 1 and 5 are immunogenic, and present their antigens at a level randomly chosen from set L_I, which is defined in (3.2). On the other hand, cells in sub-populations labelled by antigens 4, 6, 7, 8 and 10 are non-immunogenic, and present all their antigens at a lower level randomly chosen from set L_{NI}, which is defined in (3.3).

4 Results and discussion

4.1 Baseline scenario: tumour development in the absence of CD8$^+$ T cells

We first establish a baseline scenario where tumour cells grow, divide and die via the modelling rules described in Section 2.1.1, in the absence of CD8$^+$ T cells. For this case, we carry out numerical simulations for 36000 MCS, corresponding to 25 days. Figure 4 shows the growth over time of the number of tumour cells. The growth of the tumour cell number is of logistic type. Logistic growth has been used by a number of authors to model the temporal evolution of the size of solid tumours [25, 45, 47]. The carrying capacity, *i.e.* the saturation value reached by the number of tumour cells due to intra-population competition, is numerically estimated to be of about 1100 cells.
In the next subsections, we investigate the effects of CD8$^+$ T cell response to different tumours characterized by different levels of ITH. The obtained dynamics are compared with the baseline scenario. In the next simulations, we consider different compositions of the initial tumour, while the other parameters are kept constant to the values listed in Table 1 and Table 2.

4.2 The number of sub-populations of tumour cells constituting a tumour correlates with the effectiveness of the immune response

To investigate how the immune response is affected by different degrees of heterogeneity, we start by comparing two situations in which the initial tumours are characterized by different number of sub-populations of tumour cells. We consider as initial conditions *tumour-3a*, with 3 different sub-populations of tumour cells, and *tumour-7a*, with 7 different sub-populations of tumour cells, defined as in Section 3.2. For each tumour, we consider the same initial fraction of immunogenic and non-immunogenic cells, corresponding to 75% of immunogenic cells and 25% of non-immunogenic cells.

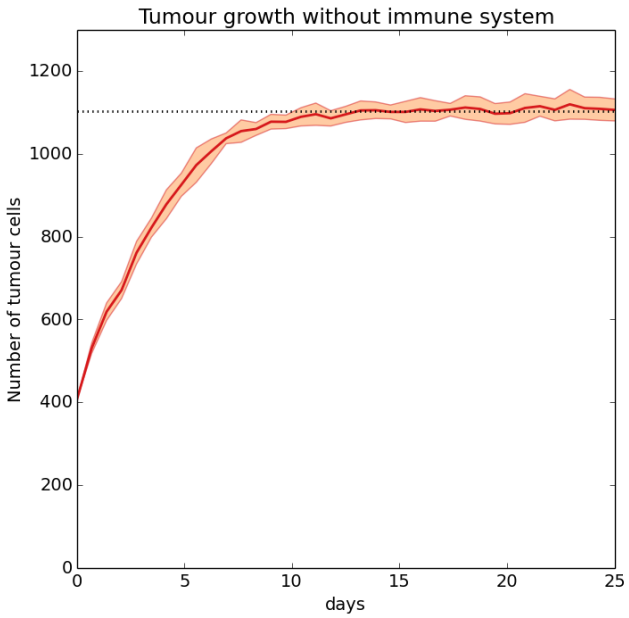

Figure 4: **Baseline scenario: tumour development in the absence of CD8$^+$ T cells.** Time evolution of the tumour cell number in the absence of CD8$^+$ T cells. The shaded area indicates $+/-$ standard deviation between 10 simulations. The black dotted line highlights a numerical estimation of the tumour cell carrying capacity.

Figure 5(a)-(c) show the time evolution of the total number of tumour cells, along with the corresponding time evolution of immunogenic and non-immunogenic cell number. Figures 5(d)-(f) also display the spatial cell distributions observed at different times of two simulations. As shown by Figure 5(a), the two tumours have similar dynamics from the beginning of simulations until day 10, with an initial increase of the cell number followed by a steep decrease. After day 10, in *tumour-3a*, the number of tumour cells continues to decrease until it reaches a low, almost constant level. Figure 5(b) and (c), along with the corresponding panel of Figure 5(f), show that, at the end of simulations, all the immunogenic cells are eliminated by the CD8$^+$ T cells, and only few non-immunogenic cells remain in the system. On the other hand, for *tumour-7a*, after day 10 the tumour cell number increases steadily over time. This dynamic leads to a final tumour size similar to the initial one. Moreover, as shown by Figure 5(b), the number of immunogenic cells decreases over time, whereas the number of non-immunogenic cells, after being initially kept under control by immune cells, increases steeply (Figure 5(c)). The related panels of Figure 5(d)-(f) show the progressive colonisation of the tumour by non-immunogenic cells.

Comparing these results with the baseline scenario of Section 4.1, for both tumours we clearly see the effects of the action of immune cells on tumour growth, which is no longer simply logistic and saturating to carrying capacity. However, the effectiveness of the immune response depends on the tumour considered. For *tumour-3a*, the immune response is efficient and almost eliminates all tumour cells. On the other hand, for *tumour-7a*, the higher heterogeneity leads to a less effective immune response and the tumour eventually grows again. These results suggest that, even if characterized by equal fractions of immunogenic and non-immunogenic cells, tumours with larger number of sub-populations of tumour cells (*i.e.* antigens) are more aggressive. This indicates that the number of sub-populations of tumour cells and antigens impact on the effectiveness of the immune response. Our outcomes are in agreement with experimental results observed in murine melanoma models presented in [78]. In this study, the induction of

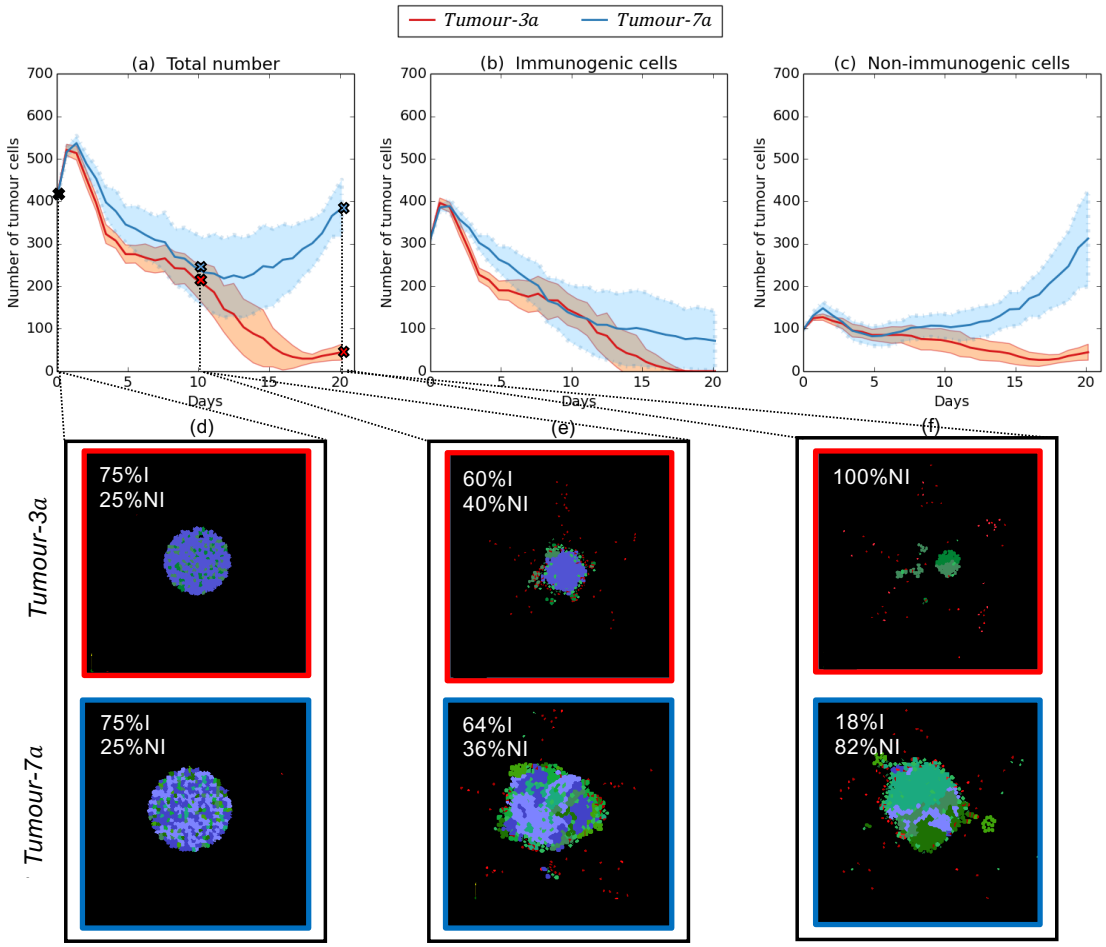

Figure 5: **The number of sub-populations constituting a tumour impacts on the effectiveness of the immune response.** Plots in panels **(a)-(c)** display the time evolution of the total tumour cell number, and the corresponding evolution of the number of immunogenic cells and non-immunogenic cells for *tumour-3a* (in red) and *tumour-7a* (in blue). Shaded areas indicate $+/-$ standard deviation between 10 simulations. For these simulations, an equal initial fraction of 75% of immunogenic cells and 25% of non-immunogenic cells was considered. Insets in panels **(d)-(f)** display an example of the spatial distribution of cells for *tumour-3a* (first row) and *tumour-7a* (second row) at different times of the simulation. Purple cells are immunogenic cells, green cells are non-immunogenic cells and red cells are $CD8^+$ T cells.

UVB-derived mutations, which lead to an increase in the number of sub-populations of tumour cells, results in aggressive tumours with decreased anti-tumour immune activity. However, when different single-cell-clone derived tumours (characterized by a unique sub-population of tumour cells) are considered, the immune system is able to effectively eradicate them.

The outcomes of our model indicate that in *tumour-3a* the presence of a low number of antigens leads to a better immune detection, enhancing the ability of the immune system to eliminate the tumour. In both tumours the immune system rapidly targets and eliminates immunogenic cells, giving a competitive advantage to non-immunogenic cells. In fact, we initially observe a reduction in the number of tumour cells. However, in *tumour-7a*, as more sub-populations of tumour cells are present, non-immunogenic cells have a better chance of escaping immune surveillance. The outcome is a weaker anti-tumour immune response. Overall, our results are in agreement with the recent hypothesis by Wolf et al. [78] that, because of increased antigenic variability, the relative expression of each antigen is weaker in tumours

composed of a larger number of sub-populations of tumour cells. In particular, clonal antigens undergo "dilution" within the tumour, and, therefore, the chance for $CD8^+$ T cells to identify immunogenic cells is reduced. This leads to a diminished ability of $CD8^+$ T cells to mount a sufficient cytotoxic response.

4.3 Different initial fractions of immunogenic and non-immunogenic cells can cause variations in anti-tumour immune response

The results discussed in the previous subsection illustrate how the effectiveness of the immune response can decreases in tumours with larger number of sub-populations of tumour cells. We investigate the effects of ITH further, focusing on the role of the fraction of immunogenic and non-immunogenic cells. We fix the number of sub-populations of tumour cells considering only *tumour-3a*, and vary the initial fraction of immunogenic and non-immunogenic cells.

The plot in Figure 6 displays the number of tumour cells remaining at the end of simulations (after 20 days), for different initial fractions of immunogenic and non-immunogenic cells. For low fractions of non-immunogenic cells ($\leq 25\%$), none or very few tumour cells survive after 20 days. On the contrary, for tumours initially composed of more than 50% of non-immunogenic cells, the number of tumour cells after 20 days is larger than the initial one. In addition, the final number of cells increases as we increase the initial fraction of non-immunogenic cells. These results suggest that the anti-tumour immune action is efficient only when the fraction of non-immunogenic cells is low compared to the fraction of immunogenic cells. Moreover, the larger the fraction of non-immunogenic cells, the weaker the immune response is.

Compared to the baseline scenario of Section 4.1, we see the effects of the immune system on tumour growth. In fact, for each scenario the number of cells at the end of simulations is lower than the tumour carrying capacity shown in Figure 4. However, for larger fractions of non-immunogenic cells, the immune response is not efficient enough to reduce the initial tumour size.

Taken together, our results qualitatively reproduce key findings of experiments performed in *in vivo* syngeneic mice tumour models [29]. The results presented in [29] indicate that a non-effective immune response may occur when the fraction of immunogenic cells in the tumour is low. Our computational results provide an explanation for such emergent behaviour. Since sub-clonal antigens are presented at a low level by the MHC-I, non-immunogenic cells trigger a poor $CD8^+$ T cell response. Thus, tumours characterized by a major fraction of non-immunogenic cells result in a weaker overall immune response. Furthermore, Gejman et al. [29] put forward the idea that the threshold fraction of immunogenic cells that is required to trigger an antigen-specific $CD8^+$ T cell response may vary depending on the antigens. In order to address this point, such a feature could be implemented in the model, for example by considering antigen presentation levels or chemotactic responses specific to each antigen.

The role of the immunogenic cell fraction within the tumour is further analysed as we observe a gap between the results obtained considering 25% and 50% of non-immunogenic cells (see Figure 6). This is investigated by performing simulations considering fractions of non-immunogenic cells between these two values. Figure 7 displays the time evolution of the number of tumour cells of 10 different simulations, corresponding to the same initial fractions of non-immunogenic cells (33%) and immunogenic cells (67%). In this case, we carry out numerical simulations for 38800 MCS (corresponding to 27 days).
With these initial conditions, we observe a large variability in the tumour-immune dynamics. In particular, Figure 7(a) shows that, in some simulations, the number of tumour cells decreases over time and only few cells remain at the end of the simulations. In other cases, after an ini-

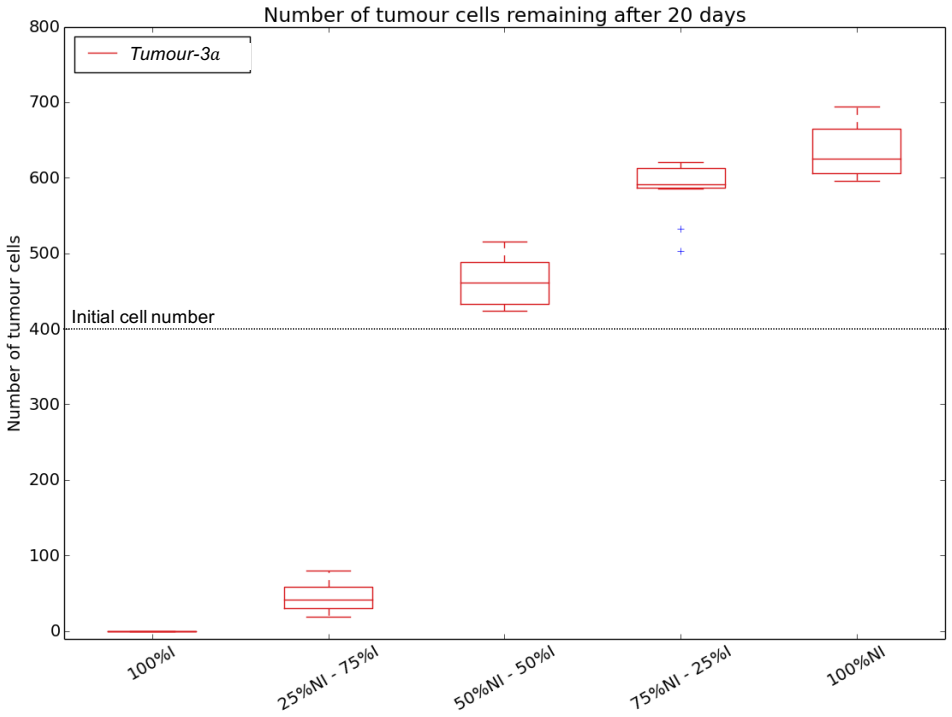

Figure 6: **Different initial fractions of immunogenic and non-immunogenic cells can cause variations in the immune response to tumour cells.** Plot displaying the number of tumour cells remaining after 20 days (28800 MCS) for different initial fractions of immunogenic and non-immunogenic cells. For these simulations, only *tumour-3a* was considered. The tumour cell numbers presented here were obtained as the average over 10 simulations and the error bars display the related standard deviation. The black dotted line highlights the number of tumour cell at the initial time of the simulations.

tial phase between day 0 and day 10 where $CD8^+$ T cells keep under control the growth of the tumour, the number of tumour cells eventually increases and the resulting final number of tumour cells is larger than the initial one. This is also illustrated by Figure 7(b), which displays a sample of the spatial cell distributions at different time of two simulations. In particular, here we show that, starting from the same initial condition, we obtain two different outcomes: in one case immune clearance occurs and tumour cells are almost entirely eliminated by the immune system; in the other case tumour cells escape immune surveillance. When immune escape occurs, in the example proposed in Figure 7(b) at day 14, immunogenic cells are surrounded by non-immunogenic cells, which hamper immune detection. This leads to a decreased influx of $CD8^+$ T cells in the tumour micro-environment and results in a weaker immune response.

These results suggest that the stochasticity which is present in cell dynamics may affect the outcomes of immune action. These results may partially explain the outcomes of earlier experimental research [17, 43], which found that responses of patients with similar tumours can vary considerably. In this regard, the use of mathematical models for identification and understanding of immune escape mechanisms in individual tumour could help advancing personalized tumour treatment.

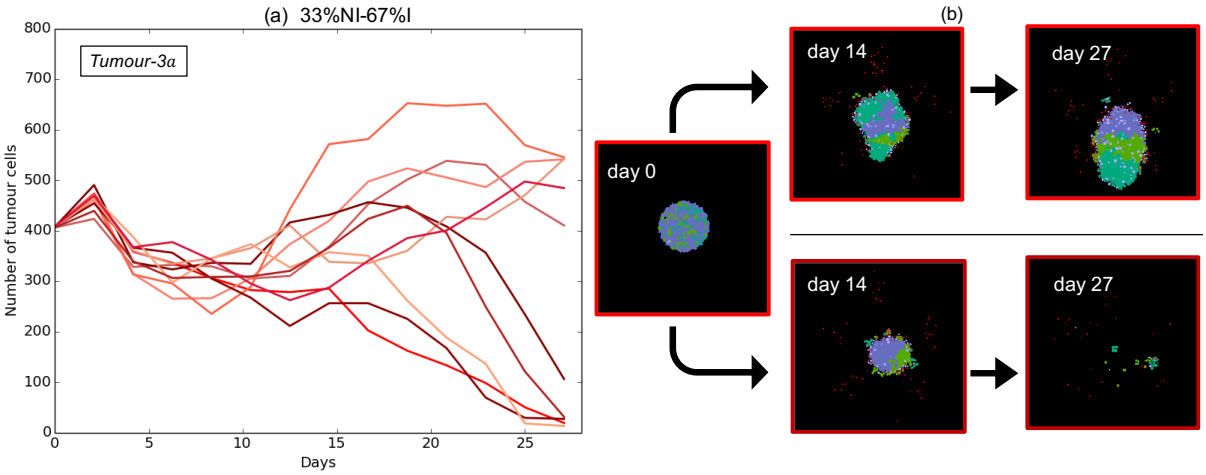

Figure 7: **Stochasticity in cell dynamics may affect the outcomes of immune action.** Plot in panel **(a)** displays the time evolution of the tumour cell number for an initial fraction of 33% of non-immunogenic cells and 67% of immunogenic cells for 10 runs of simulations. For these simulations, only *tumour-3a* was considered. The insets in panel **(b)** show an example of the observed spatial distributions of cells corresponding to different times of two simulations.

4.4 Both the number of sub-populations of tumour cells constituting a tumour and the fraction of immunogenic and non-immunogenic cells affect the effectiveness of the immune response

So far, we have investigated with our model the effects of ITH on immune response by varying independently the number of sub-populations of tumour cells constituting a tumour and the fraction of immunogenic and non-immunogenic cells. Now, we study their combined effect in mediating tumour growth. We consider as initial conditions *tumour-3a* and *tumour-7a*, characterized by different numbers of sub-populations of tumour cells, and for different initial fractions of immunogenic and non-immunogenic cells.

Figure 8 displays the time evolution of the total number of cells for different initial tumour compositions, and compares the number of immunogenic and non-immunogenic cells at the end of simulations with respect to the initial one. As shown by Figure 8(a1), the immune system is able to completely eradicate the tumour only when it is initially composed of 100% of immunogenic cells, independently of the number of sub-populations of tumour cells. When the initial tumour is made of 25% of non-immunogenic cells, Figure 8(b1) show that the two tumours have different dynamics. In particular, as already observed in the results presented in Section 4.2, the number of cells in *tumour-3a* decreases over time until the end of the simulations, while the number of cells in *tumour-7a*, after an initial decrease, steadily increases until the end of the simulations. Finally, when tumours are initially composed of more than 50% of non-immunogenic cells, similarly to the baseline scenario of Section 4.1, they follow a logistic growth, except for an initial decrease shown by Figure 8(c1). For both tumours, the tumour cell number eventually saturates at a certain value (see Figure 8(c1)-(e1)). In these cases, the saturation value of the number of tumour cells is larger than the initial tumour cell number. Moreover, the saturation value attained increases as we increase the level of heterogeneity of the tumour (respectively, the number of sub-populations of tumour cells and the fraction of non-immunogenic cells). Such results indicate that in these cases $CD8^+$ T cells are present in the tumour micro-environment but do not produce an effective immune response. Persistent antigen presentation has been proven to cause continuous TCR stimulation that could directly

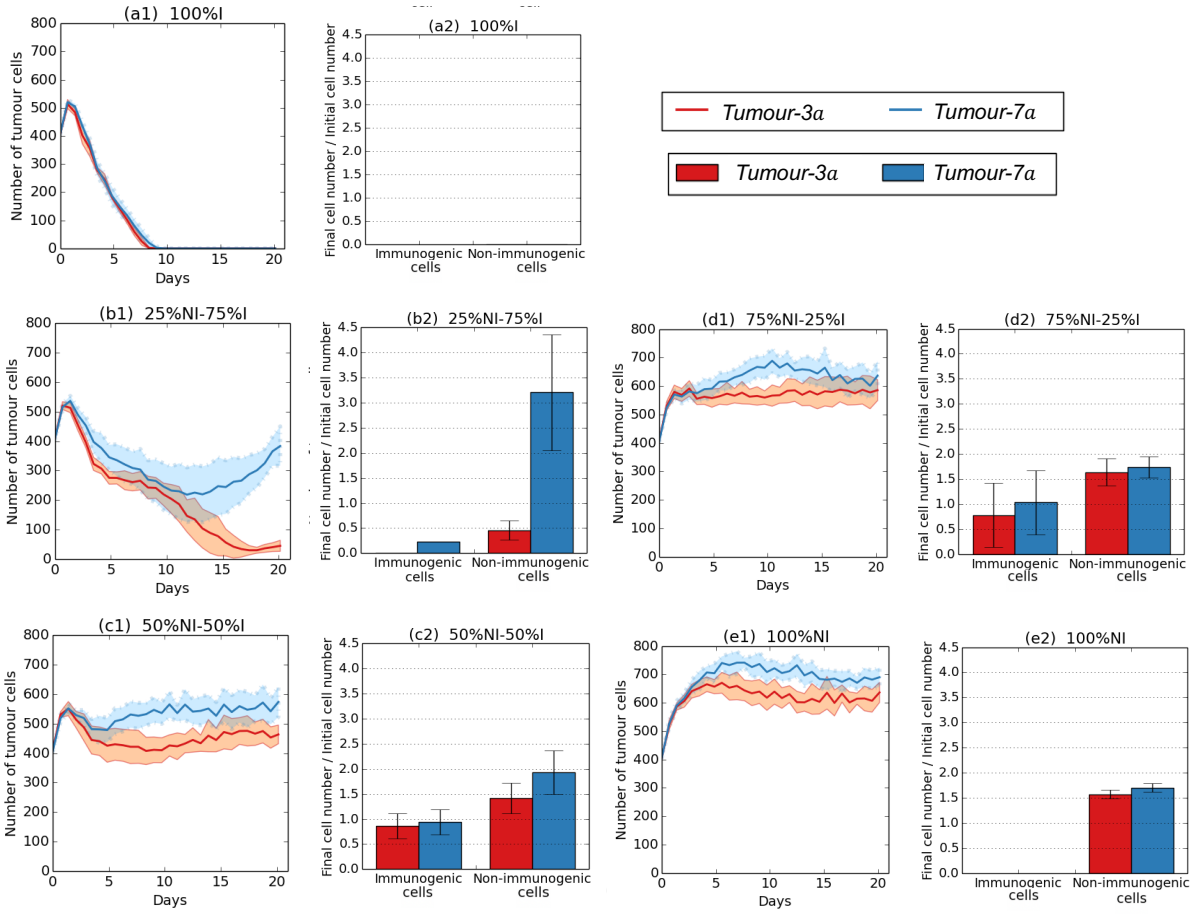

Figure 8: **Both the number of sub-populations constituting a tumour and the fraction of non-immunogenic cells affect the effectiveness of the immune response.** Plots in panel **(a1)-(e1)** display the time evolution of the tumour cell number for *tumour-3a* (in red) and *tumour-7a* (in blue). In both tumours, from **(a1)** to **(e1)** the initial fraction of non-immunogenic cells is increased. Shaded areas indicate $+/-$ standard deviation between 10 simulations. Plots in panel **(a2)-(e2)** display the corresponding average number of immunogenic and non-immunogenic cells at the end of simulations with respect to the initial one. The error lines represent the standard deviation between 10 simulations.

induce $CD8^+$ T cell dysfunction and exhaustion [79, 80]. The model presented in this work does not include this aspect, but it could be easily extended to do so.

The outcomes of our model recapitulate the main results of in *in vivo* clonal mixing experiments in mice models presented by Wolf et al. [78], who studied the combined effect of these two characteristics of ITH in mediating tumour growth and eradication. Wolf and collaborators have demonstrated that tumours with increased number of clones and large genetic diversity are more aggressive. In our model, the number of clones can be linked to the number of sub-populations of tumour cells, while genetic diversity may be linked to the immunogenicity of the tumour. Moreover, our findings are in agreement with an experimental work indicating that patients whose tumours are highly heterogeneous have increased levels of relapse after an initial response to immunotherapy and worse survival expectations than patients with more homogeneous tumours [59].

We next analyse the evolution over time of immunogenic and non-immunogenic cells. When tumours are initially composed of 25% of non-immunogenic cells, Figure 8(b2) shows

that the two tumours evolve in different ways. While the number of non-immunogenic cells is considerably reduced in *tumour-3a*, the final number of non-immunogenic cells increases up to four times its initial number in *tumour-7a*. On the other hand, when tumours are initially composed of more than 50% of non-immunogenic cells, independently of the tumour considered, we observe a similar trend in the evolution of immunogenic and non-immunogenic cells (see Figure 8(c2)-(e2)). In particular, for both tumour types, the number of immunogenic cells tends to remain stable or decreases slightly. On the other hand, the number of non-immunogenic cells increases and grows to up to twice its initial value.
These results suggest that, beyond a certain non-immunogenic cell fraction threshold, the immune system becomes inefficient in both tumour types independently of the number of sub-populations of tumour cells. Moreover, they suggest that the selective pressure of the immune response can lead to more aggressive tumours, characterized by larger fractions of non-immunogenic cells. In this regard, our results follow the same behaviour of previous experimental works demonstrating that, under cancer therapeutics (*e.g.* chemotherapy or radiotherapy), the population of tumour cells is exposed to the selective stress induced by the treatment [34, 38, 75]. Therefore, more resistant cells acquire a competitive advantage over more sensitive cells and induce a weaker response to treatment in the long run. The resulting outcome is a more aggressive tumour, which may ultimately grow again [63].

5 Conclusions

The number of sub-populations of tumour cells constituting a tumour and the fraction of immunogenic and non-immunogenic cells within it are two major components of ITH, and play a key role in the immune response against solid tumours. Mathematical models make it possible to asses the influence of these two components of ITH on anti-tumour immunity in a controlled manner.
In this work, we have presented a spatially explicit stochastic individual-based model of the interaction dynamics between $CD8^+$ T cells and tumour cells, and we have investigated how ITH affects the anti-tumour immune response.
Our numerical results show that the number of sub-populations of tumour cells constituting a tumour can have a crucial impact upon the outcome of the immune response (Figure 5). In the scenario of a tumour characterized by a low number of sub-populations of tumour cells, immune clearance can occur. Conversely, when the initial tumour is composed of a larger number of sub-populations, the tumour may be able to escape immune recognition and ultimately grow again. In this case, our results demonstrate that, in more heterogeneous tumours, tumour cells could have a better chance of escaping immune surveillance because clonal antigens undergo "dilution" within the tumour relative to other antigens, diminishing the ability of $CD8^+$ T cells to mount a sufficient cytotoxic response.
The outcomes of our model support the idea that varying the initial fraction of immunogenic and non-immunogenic cells leads to variations on the effectiveness of the immune response and results in distinct scenarios, from immune clearance of the tumour to immune escape (Figure 6). We have also observed that for certain intermediate fractions of immunogenic and non-immunogenic cells, stochasticity in cell dynamics plays an important role, and can lead both scenarios close to tumour eradication and to scenarios where a large number of tumour cells persists over time (Figure 7).
We have also studied the effects of ITH on anti-tumour immune response by varying both the number of sub-populations of tumour cells and the initial fraction of immunogenic and non-immunogenic cells (Figure 8). For equal fraction of immunogenic and non-immunogenic cells, tumours with increased number of sub-populations of tumour cells are more aggressive than tumours with lower number of sub-populations of tumour cells. However, beyond a certain threshold value of the fraction of non-immunogenic cells, the immune system becomes

inefficient against both types of tumours, independently of the number of sub-populations of tumour cells. In addition, we found that increasing initial fractions of non-immunogenic cells always led to a less effective $CD8^+$ T cell response. When the tumours are not eradicated, the final fraction of non-immunogenic cells is larger than the initial one. This suggests that the immune system may act as a bottleneck which selects and eliminates immunogenic cells, thus allowing the tumours to escape immune regulation.
In summary, our findings demonstrate the importance of ITH as a possible predictor of the outcome of immune action. Our results support the idea that patients with tumours bearing few clonal antigens are expected to be more likely to exhibit a durable benefit from immune response than patients with heterogeneous tumours characterized by many different sub-clonal antigens [59]. On the other hand, our results disbelieve the fact that highly heterogeneous tumours, characterized by the expression of many different antigens, can enhance the efficacy of immune response. In fact, our results indicate that excessive antigen heterogeneity may, conversely, actively impair anti-tumour $CD8^+$ T cell immune response. This is also supported by a recent clinical work which found that excessive mutagenesis, directed to enhance the tumour mutational burden, may decrease the efficacy of immunotherapy [78].

The current version of our model can be developed further in several ways. We could incorporate extended aspects of the tumour micro-environment, such as the expression of immunosuppressive factors (*e.g.* PD1 or CTLA4), which affect the effectiveness of anti-tumour immune response. In fact, these inhibitory factors induce the exhaustion of $CD8^+$ T cells in the tumour micro-environment impairing the immune response [40, 77]. The inclusion of $CD8^+$ T cell exhaustion caused by inhibitory factors could give further explanations for other mechanisms of immune escape. The exhaustion mechanism could be included in the model by, for example, altering the value of the parameter governing the efficiency of the $CD8^+$ T cell population in eliminating tumour cells.
The spatial dimension and the flexibility of our model would also allow for the study of the spatial distribution of $CD8^+$ T cells within the tumour and the role of immune infiltration on the tumour dynamics [27]. Moreover, by posing the model on a 3D domain, a deeper understanding of the spatial dynamics of tumour-immune interactions could be achieved.
Finally, from a modelling point of view, although more tailored to capture fine details of the dynamics of single cells, individual-based models are not amenable to analytical studies, which may support a more in-depth theoretical understanding of the application problems under study. For this reason, it would be useful to derive a continuum version of our model by using mean filed methods similar to those employed in [5, 18, 64].
In perspective, our model may be used to assess different levels of ITH as biomarkers for comparing and predicting outcomes in tumour treatment. Coupling the model with tumour biopsies from patients could offer insight into potential outcomes of treatments. Finally, our model may be a promising tool to explore therapeutic strategies designed to decrease tumour heterogeneity and improve the overall anti-tumour immune response.

CRediT authorship contribution statement

Emma Leschiera: Conceptualization, Methodology, Software, Formal analysis, Investigation, Visualization, Writing - original draft. **Tommaso Lorenzi**: Conceptualization, Methodology, Writing - Review & Editing, Supervision. **Shensi Shen**: Conceptualization, Methodology, Resources, Writing - Review & Editing. **Luis Almeida**: Conceptualization, Methodology, Writing - Review & Editing, Supervision. **Chloe Audebert**: Conceptualization, Methodology, Formal analysis, Validation, Visualization, Writing - original draft, Supervision.

Acknowledgments

The authors are grateful to Jacqueline Marvel for sharing her knowledge on the immune response.
E.L. has received funding from the European Research Council (ERC) under the European Union's Horizon2020 research and innovation programme (grant agreement No 740623).
T.L. gratefully acknowledges support of the MIUR grant "Dipartimenti di Eccellenza 2018-2022".

A Details of computational model

The individual-based model has been numerically solved using the multicellular modelling environment CompuCell3D [39]. This software is an open source solver, which uses a Cellular Potts model [33] (also known as CPM, or Glazier-Graner-Hogeweg model). In Cellular Potts models, biological cells are treated as discrete entities represented as a set of lattice sites, each with characteristic values of area, perimeter, and intrinsic motility on a regular lattice. Interaction descriptions and dynamics between cells are modelled by means of the effective energy of the system. This determines many characteristics such as cell size, motility, adhesion strength and the reaction to gradients of chemotactic fields. During a simulation, each cell will attempt to extend its boundaries, through a series of index-copy attempts, in order to minimise the effective energy. The success of the index copy attempt is dependent upon probabilistic rules which take into account the change in energy.

A.1 Cell types

In Cellular Potts models, cells are uniquely identified with an index $\sigma(i)$ on each lattice site i, with i a vector of integers occupying lattice site i. Each cell in the model has a type $\tau(\sigma(i))$, which determines its properties, and the processes and interactions in which it participate. In our model, to characterise the different sub-populations of tumour cells, we define as many types of tumour cells as sub-populations of tumour cells. Moreover, $CD8^+$ T cells have as many types as TCRs considered for the simulation, which corresponds also to the number of antigens considered. Note that, technically, the extracellular medium is also considered as a cell of type medium.

A.2 Cellular dynamics

The effective energy is the basis for operation of all Cellular Potts models, including CompuCell3D [39], because it determines the interactions between cells (including the extracellular medium). Configurations evolve to minimize the effective energy H of the system, defined as

$$H = \underbrace{\sum_{i,j} J(\tau(\sigma_i),\tau(\sigma_j))(1-\delta(\sigma_i,\sigma_j))}_{\text{boundary energy}} + \underbrace{\sum_{\sigma}\left[\lambda_{area}(\sigma)(a(\sigma)-A_t(\sigma))^2\right]}_{\text{area constraint}} + \underbrace{\sum_{\sigma}\left[\lambda_{per}(\sigma)(p(\sigma)-P_t(\sigma))^2\right]}_{\text{perimeter constraint}} \tag{A.1}$$

The most important component of the effective energy equation is the boundary energy, which governs the adhesion of cells. The boundary energy $J(\tau(\sigma_i),\tau(\sigma_j))$ describes the contact energy between two cells σ_i and σ_j of types $\tau(\sigma_i)$ and $\tau(\sigma_j)$. It is calculated by the sum over all neighbouring pixels i and j that form the boundary between two cells. Thanks to the term $(1-\delta(\sigma_i,\sigma_j))$, the boundary energy contribution is considered only between lattice sites belonging to two different cells. The second and third terms represent respectively a cell-area and cell-perimeter constraint. In particular, $a(\sigma)$ and $p(\sigma)$ are the surface area and perimeter

of the cell σ, $A_t(\sigma)$ and $P_t(\sigma)$ are the cell's target surface area and perimeter and $\lambda_{area}(\sigma)$ and $\lambda_{per}(\sigma)$ are an area and perimeter constraint coefficient.

The cell configuration evolves through lattice-site copy attempts. To begin an index-copy attempt, the algorithm randomly selects a lattice site to be a target pixel i, and a neighbouring lattice site to be a source pixel i'. If the source and target pixels belong to the same cell (*i.e.* if $\sigma(i) = \sigma(i')$), they do not need to attempt an lattice-site copy and thus the effective energy will not be calculated. Otherwise, an attempt will be made to switch the target pixel as the source pixel, thereby increasing the surface area of the source cell and decreasing the surface area of the target cell.

The algorithm computes $\Delta H = H - H'$, with H the effective energy of the system and H' the effective energy if the copy occurs. Then, it sets $\sigma(i) = \sigma(i')$ with probability $P(\sigma(i) \to \sigma(i'))$, given by:

$$P(\sigma(i) \to \sigma(i')) = \begin{cases} 1 & : \quad \Delta H \leq 0 \\ \exp^{-\frac{\Delta H}{T_m}} & : \quad \Delta H > 0. \end{cases} \tag{A.2}$$

The change in effective energy ΔH evaluate the energy cost of such a copy and parameter T_m determines the stochasticity of accepted copy attempts. The unit of simulation time is the Monte Carlo step (MCS).

A.3 Subcellular dynamics and chemotaxis

In our model we simulate CD8$^+$ T cell chemotaxis toward tumour cells, defined as the cell motion induced by a presence of a chemical. In CompuCell3D [39], chemotaxis is obtained biasing the cell's motion up or down a field gradient by adding a term ΔH_{chem} in the calculated effective-energy change ΔH used in the acceptance function (A.2). For a field $c(i)$:

$$\Delta H_{chem} = -\lambda_{chem}(c(i) - c(i')) \tag{A.3}$$

where $c(i)$ is the chemical field at the index-copy target pixel i, $c(i')$ the field at the index-copy source pixel i', and λ_{chem} the strength and direction of chemotaxis.

The change in concentration of the chemical field c is obtained by solving a reaction-diffusion equation of the following general form:

$$\frac{\partial c}{\partial t} = D\nabla^2 c - \gamma c + S \tag{A.4}$$

where D, γ and S denote the diffusion constant, decay constant and secretion rates of the field, respectively. These three parameters may vary with position and cell-lattice configuration, and thus be a function of cell σ and pixel i.

B Model parameters

The individual-based model is parametrised using parameter values obtained from published biological data wherever possible. We use a 2D squared spatial domain with 400×400 lattice sites (pixels). We assume that a pixel of the domain corresponds to 3×3 μm^2. As the CD8$^+$ T cell diameter is estimated to be between 10 μm and 12 μm [28, 32], the initial size of a CD8$^+$ T cell is 4×4 pixels. A tumour cell diameter is estimated to be about 20 μm [19], therefore we assume that each newly divided tumour cell is made of 5×5 pixels. In addition, the maximum CD8$^+$ T cell migration speed measured in the simulation is around 10 pixels / 100 MCS. Therefore, using the CD8$^+$ T cell migration measurements *in vivo* (2-25 $\mu m/min$, see Miller et al. [62]) we choose 1 MCS $\sim$ 1 minute as a time scale. The parameters for the Cellular Potts model are listed in Table 1, while all the other parameters with their related references are listed in Table 2. Files to run a simulation example with Compucell3D software are available at: https://plmlab.math.cnrs.fr/audebert/cc3dmodeltumourcd8.

Table 1: Parameter values used to implement the Cellular Potts model. Energies, temperature and constrains are dimensionless parameters.

Phenotype	Symbol	Description	Value	Reference
Domain	$\Delta x, \Delta y$	Domain spacing in the x or y direction	1 Pixel = 3 × 3 μm^2	
	Δt	Time-step	1 MCS = 1 min	
	t_f	Final time	20 (*days*)	
CC3D	J_{MT}	Contact energy tumour cells-medium	50	
	J_{MC}	Contact energy CD8$^+$ T cells-medium	50	
	J_{CT}	Contact energy CD8$^+$ T cells-tumour cells	20	
	J_{TT}	Contact energy tumour cells-tumour cells	110	
	J_{CC}	Contact energy CD8$^+$ T cells-CD8$^+$ T cells	1000	
	d_T	Tumour cell diameter	20-40 (μm)	[32]
	d_C	CD8$^+$ cell diameter	12 (μm)	[28]
	λ_{area}	Tumour cell area constrain	10	
	λ_{per}	Tumour cell perimeter constrain	10	
	T_m	Temperature	10	
	λ_{chem}	Strength and direction of chemotaxis	50	

References

[1] G. Aguadé-Gorgorió and R. Solé. Tumour neoantigen heterogeneity thresholds provide a time window for combination immunotherapy. *Journal of the Royal Society Interface*, 17 (171):20200736, 2020.

[2] A. A. Alizadeh, V. Aranda, A. Bardelli, C. Blanpain, C. Bock, C. Borowski, C. Caldas, A. Califano, M. Doherty, M. Elsner, et al. Toward understanding and exploiting tumor heterogeneity. *Nature medicine*, 21(8):846, 2015.

[3] V. Anagnostou, K. N. Smith, P. M. Forde, N. Niknafs, R. Bhattacharya, J. White, T. Zhang, V. Adleff, J. Phallen, N. Wali, et al. Evolution of neoantigen landscape during immune checkpoint blockade in non–small cell lung cancer. *Cancer discovery*, 7(3):264–276, 2017.

[4] A. Anderson and K. Rejniak. *Single-cell-based models in biology and medicine*. Springer Science & Business Media, 2007.

[5] A. Ardaševa, A. R. Anderson, R. A. Gatenby, H. M. Byrne, P. K. Maini, and T. Lorenzi. Comparative study between discrete and continuum models for the evolution of competing phenotype-structured cell populations in dynamical environments. *Physical Review E*, 102(4):042404, 2020.

[6] A. D. Asatryan and N. L. Komarova. Evolution of genetic instability in heterogeneous tumors. *Journal of theoretical biology*, 396:1–12, 2016.

[7] K. Atsou, F. Anjuère, V. M. Braud, and T. Goudon. A size and space structured model describing interactions of tumor cells with immune cells reveals cancer persistent equilibrium states in tumorigenesis. *Journal of Theoretical Biology*, 490:110163, 2020.

[8] V. P. Balachandran, M. Łuksza, J. N. Zhao, V. Makarov, J. A. Moral, R. Remark, B. Herbst, G. Askan, U. Bhanot, Y. Senbabaoglu, et al. Identification of unique neoantigen qualities in long-term survivors of pancreatic cancer. *Nature*, 551(7681):512–516, 2017.

Table 2: Parameter values used in numerical simulations.

Phenotype	Description	Value	Reference
Tumour	Initial number	$N_T(0) = 400$	
	Index identifier	$n = 1, \ldots, N_T(t)$	
	Lifespan	$\mathcal{U}_{[3,7]}$ (*days*)	[32]
	Growth rate	$\mathcal{U}_{[0.015,0.02]}$ (*pixel/min*)	
	Mean cycle time	24 (*hours*)	[32]
	Rate of death due to competition between tumour cells	3.8×10^{-7} (*1/min*)	
	Antigen profile	$A = (a_1, \ldots, a_f)$	
	Clonal antigen profile	$A_C \subset A$	
	Sub-clonal antigen profile	$A_{SC} \subset A$	
	Range of value of antigen presentation for clonal cells	$L_I = \{\frac{1}{6}, \frac{2}{6}, \frac{3}{6}, \frac{4}{6}, \frac{5}{6}, 1\}$	
	Range of value of antigen presentation for sub-clonal cells	$L_{NI} = \{\frac{5}{100}, \frac{10}{100}, \frac{15}{100}, \frac{20}{100}, \frac{25}{100}, \frac{30}{100}\}$	
	Antigen	$a_i \in A$	
	Level of presentation of antigen a_i of tumour cell n	$l^n_{a_i} \in [0, 1]$	
CD8$^+$ T cells	Total number at time t	$N_C(t) \geq 0$	
	Index identifier	$m = 1, \ldots, N_C(t)$	
	Influx rate	$p(t) = C_1 \times S^{tot}_a(t)$ $C_1 = 2 \times 10^{-5}$ (*min/mol*)	
	Lifespan	$\mathcal{U}_{[2.5,3.5]}$ (*days*)	[32]
	Migration speed	2 - 25 (μm/*min*)	[28]
	Engagement time	6 (*hours*)	[19]
	TCR-recognition probability	$r = 0.901$	
Chemoattractant	Concentration	$c_{a_i} \geq 0$ (*mol/pixel*)	
	Total amount secreted	$S^{tot}_{a_i} \geq 0$ (*mol/min*)	
	Diffusion	$D = 7 \times 10^{-1}$ (*pixel*^{2}*/min*)	
	Secretion	$s^n_{a_i} = C_2 \times l^n_a$ (*mol/min/pixel*) $C_2 = 10$ (*mol/min/pixel*)	
	Decay	$\gamma = 3 \times 10^{-4}$ (*1/min*)	
	Initial concentration	$c^{init}_{a_i} = 0.5(280 - \sqrt{(x-200)^2 + (y-200)^2})$	

[9] R. Basu, B. M. Whitlock, J. Husson, A. Le Floc'h, W. Jin, A. Oyler-Yaniv, F. Dotiwala, G. Giannone, C. Hivroz, N. Biais, et al. Cytotoxic t cells use mechanical force to potentiate target cell killing. *Cell*, 165(1):100–110, 2016.

[10] A. Boissonnas, L. Fetler, I. S. Zeelenberg, S. Hugues, and S. Amigorena. In vivo imaging of cytotoxic t cell infiltration and elimination of a solid tumor. *The Journal of experimental medicine*, 204(2):345–356, 2007.

[11] A. Bouchnita, F.-E. Belmaati, R. Aboulaich, M. J. Koury, and V. Volpert. A hybrid computation model to describe the progression of multiple myeloma and its intra-clonal heterogeneity. *Computation*, 5(1):16, 2017.

[12] B. Breart, F. Lemaître, S. Celli, and P. Bousso. Two-photon imaging of intratumoral cd8+ t cell cytotoxic activity during adoptive t cell therapy in mice. *The Journal of clinical investigation*, 118(4):1390–1397, 2008.

[13] F. Bubba, T. Lorenzi, and F. R. Macfarlane. From a discrete model of chemotaxis with volume-filling to a generalized patlak–keller–segel model. *Proceedings of the Royal Society A*, 476(2237):20190871, 2020.

[14] Í. Caramalho, M. Faroudi, E. Padovan, S. Müller, and S. Valitutti. Visualizing

ctl/melanoma cell interactions: multiple hits must be delivered for tumour cell annihilation. *Journal of cellular and molecular medicine*, 13(9b):3834–3846, 2009.

[15] T. A. Chan, M. Yarchoan, E. Jaffee, C. Swanton, S. A. Quezada, A. Stenzinger, and S. Peters. Development of tumor mutation burden as an immunotherapy biomarker: utility for the oncology clinic. *Annals of Oncology*, 30(1):44–56, 2019.

[16] M. A. Chaplain, T. Lorenzi, and F. R. Macfarlane. Bridging the gap between individual-based and continuum models of growing cell populations. *Journal of mathematical biology*, 80(1):343–371, 2020.

[17] D. S. Chen and I. Mellman. Elements of cancer immunity and the cancer–immune set point. *Nature*, 541(7637):321–330, 2017.

[18] R. H. Chisholm, T. Lorenzi, L. Desvillettes, and B. D. Hughes. Evolutionary dynamics of phenotype-structured populations: from individual-level mechanisms to population-level consequences. *Zeitschrift für angewandte Mathematik und Physik*, 67(4):1–34, 2016.

[19] C. Christophe, S. Müller, M. Rodrigues, A.-E. Petit, P. Cattiaux, L. Dupré, S. Gadat, and S. Valitutti. A biased competition theory of cytotoxic t lymphocyte interaction with tumor nodules. *PloS one*, 10(3), 2015.

[20] P. G. Coulie, B. J. Van den Eynde, P. Van Der Bruggen, and T. Boon. Tumour antigens recognized by t lymphocytes: at the core of cancer immunotherapy. *Nature Reviews Cancer*, 14(2):135–146, 2014.

[21] L. G. de Pillis and A. Radunskaya. A mathematical model of immune response to tumor invasion. In *Computational fluid and solid mechanics 2003*, pages 1661–1668. Elsevier, 2003.

[22] L. G. de Pillis, D. G. Mallet, and A. E. Radunskaya. Spatial tumor-immune modeling. *Computational and Mathematical Methods in medicine*, 7(2-3):159–176, 2006.

[23] M. Delitala and T. Lorenzi. Recognition and learning in a mathematical model for immune response against cancer. *Discrete & Continuous Dynamical Systems-B*, 18(4):891, 2013.

[24] P. J. Delves and I. M. Roitt. The immune system. *New England journal of medicine*, 343(1): 37–49, 2000.

[25] D. Drasdo and S. Höhme. Individual-based approaches to birth and death in avascu1ar tumors. *Mathematical and Computer Modelling*, 37(11):1163–1175, 2003.

[26] F. L. Fennemann, I. J. M. de Vries, C. G. Figdor, and M. Verdoes. Attacking tumors from all sides: Personalized multiplex vaccines to tackle intratumor heterogeneity. *Frontiers in Immunology*, 10:824, 2019.

[27] J. Galon and D. Bruni. Approaches to treat immune hot, altered and cold tumours with combination immunotherapies. *Nature Reviews Drug Discovery*, 18(3):197–218, 2019.

[28] X. Gao, C. Arpin, J. Marvel, S. A. Prokopiou, O. Gandrillon, and F. Crauste. Il-2 sensitivity and exogenous il-2 concentration gradient tune the productive contact duration of cd8+ t cell-apc: a multiscale modeling study. *BMC systems biology*, 10(1):77, 2016.

[29] R. S. Gejman, A. Y. Chang, H. F. Jones, K. DiKun, A. A. Hakimi, A. Schietinger, and D. A. Scheinberg. Rejection of immunogenic tumor clones is limited by clonal fraction. *Elife*, 7: e41090, 2018.

[30] G. Germano, S. Lamba, G. Rospo, L. Barault, A. Magrì, F. Maione, M. Russo, G. Crisafulli, A. Bartolini, G. Lerda, et al. Inactivation of dna repair triggers neoantigen generation and impairs tumour growth. *Nature*, 552(7683):116–120, 2017.

[31] A. Ghaffarizadeh, R. Heiland, S. H. Friedman, S. M. Mumenthaler, and P. Macklin. Physicell: an open source physics-based cell simulator for 3-d multicellular systems. *PLoS computational biology*, 14(2):e1005991, 2018.

[32] C. Gong, O. Milberg, B. Wang, P. Vicini, R. Narwal, L. Roskos, and A. S. Popel. A computational multiscale agent-based model for simulating spatio-temporal tumour immune response to pd1 and pdl1 inhibition. *Journal of the Royal Society Interface*, 14(134):20170320, 2017.

[33] F. Graner and J. A. Glazier. Simulation of biological cell sorting using a two-dimensional extended potts model. *Physical review letters*, 69(13):2013, 1992.

[34] M. Greaves and C. C. Maley. Clonal evolution in cancer. *Nature*, 481(7381):306–313, 2012.

[35] M. M. Gubin, X. Zhang, H. Schuster, E. Caron, J. P. Ward, T. Noguchi, Y. Ivanova, J. Hundal, C. D. Arthur, W.-J. Krebber, et al. Checkpoint blockade cancer immunotherapy targets tumour-specific mutant antigens. *Nature*, 515(7528):577–581, 2014.

[36] T. H. Harris, E. J. Banigan, D. A. Christian, C. Konradt, E. D. T. Wojno, K. Norose, E. H. Wilson, B. John, W. Weninger, A. D. Luster, et al. Generalized lévy walks and the role of chemokines in migration of effector cd8+ t cells. *Nature*, 486(7404):545–548, 2012.

[37] M. D. Hellmann, T. Nathanson, H. Rizvi, B. C. Creelan, F. Sanchez-Vega, A. Ahuja, A. Ni, J. B. Novik, L. M. Mangarin, M. Abu-Akeel, et al. Genomic features of response to combination immunotherapy in patients with advanced non-small-cell lung cancer. *Cancer cell*, 33(5):843–852, 2018.

[38] Y. Iwasa, M. A. Nowak, and F. Michor. Evolution of resistance during clonal expansion. *Genetics*, 172(4):2557–2566, 2006.

[39] J. A. Izaguirre, R. Chaturvedi, C. Huang, T. Cickovski, J. Coffland, G. Thomas, G. Forgacs, M. Alber, G. Hentschel, S. A. Newman, et al. Compucell, a multi-model framework for simulation of morphogenesis. *Bioinformatics*, 20(7):1129–1137, 2004.

[40] Y. Jiang, Y. Li, and B. Zhu. T-cell exhaustion in the tumor microenvironment. *Cell death & disease*, 6(6):e1792–e1792, 2015.

[41] J. N. Kather, J. Poleszczuk, M. Suarez-Carmona, J. Krisam, P. Charoentong, N. A. Valous, C.-A. Weis, L. Tavernar, F. Leiss, E. Herpel, et al. In silico modeling of immunotherapy and stroma-targeting therapies in human colorectal cancer. *Cancer research*, 77(22):6442–6452, 2017.

[42] J. Kim and D. S. Chen. Immune escape to pd-l1/pd-1 blockade: seven steps to success (or failure). *Annals of Oncology*, 27(8):1492–1504, 2016.

[43] P. S. Kim and P. P. Lee. Modeling protective anti-tumor immunity via preventative cancer vaccines using a hybrid agent-based and delay differential equation approach. *PLoS Comput Biol*, 8(10):e1002742, 2012.

[44] R. Kim. Cancer immunoediting: from immune surveillance to immune escape. *Cancer Immunotherapy*, pages 9–27, 2007.

[45] D. Kirschner and J. C. Panetta. Modeling immunotherapy of the tumor–immune interaction. *Journal of mathematical biology*, 37(3):235–252, 1998.

[46] M. Kolev, S. Nawrocki, and B. Zubik-Kowal. Numerical simulations for tumor and cellular immune system interactions in lung cancer treatment. *Communications in nonlinear science and numerical simulation*, 18(6):1473–1480, 2013.

[47] V. A. Kuznetsov, I. A. Makalkin, M. A. Taylor, and A. S. Perelson. Nonlinear dynamics of immunogenic tumors: parameter estimation and global bifurcation analysis. *Bulletin of mathematical biology*, 56(2):295–321, 1994.

[48] E. Lakatos, M. J. Williams, R. O. Schenck, W. C. Cross, J. Househam, B. Werner, C. Gatenbee, M. Robertson-Tessi, C. P. Barnes, A. R. Anderson, et al. Evolutionary dynamics of neoantigens in growing tumours. *BioRxiv*, page 536433, 2019.

[49] T. Lorenzi, R. H. Chisholm, M. Melensi, A. Lorz, and M. Delitala. Mathematical model reveals how regulating the three phases of t-cell response could counteract immune evasion. *Immunology*, 146(2):271–280, 2015.

[50] T. Lorenzi, R. H. Chisholm, and J. Clairambault. Tracking the evolution of cancer cell populations through the mathematical lens of phenotype-structured equations. *Biology direct*, 11(1):1–17, 2016.

[51] M. Łuksza, N. Riaz, V. Makarov, V. P. Balachandran, M. D. Hellmann, A. Solovyov, N. A. Rizvi, T. Merghoub, A. J. Levine, T. A. Chan, et al. A neoantigen fitness model predicts tumour response to checkpoint blockade immunotherapy. *Nature*, 551(7681):517–520, 2017.

[52] F. R. Macfarlane, T. Lorenzi, and M. A. Chaplain. Modelling the immune response to cancer: an individual-based approach accounting for the difference in movement between inactive and activated t cells. *Bulletin of mathematical biology*, 80(6):1539–1562, 2018.

[53] F. R. Macfarlane, M. A. Chaplain, and T. Lorenzi. A stochastic individual-based model to explore the role of spatial interactions and antigen recognition in the immune response against solid tumours. *Journal of theoretical biology*, 480:43–55, 2019.

[54] D. G. Mallet and L. G. De Pillis. A cellular automata model of tumor–immune system interactions. *Journal of theoretical biology*, 239(3):334–350, 2006.

[55] A. Matzavinos and M. A. Chaplain. Travelling-wave analysis of a model of the immune response to cancer. *Comptes rendus biologies*, 327(11):995–1008, 2004.

[56] A. Matzavinos, M. A. Chaplain, and V. A. Kuznetsov. Mathematical modelling of the spatio-temporal response of cytotoxic t-lymphocytes to a solid tumour. *Mathematical Medicine and Biology*, 21(1):1–34, 2004.

[57] K.-A. McDonald, T. Kawaguchi, Q. Qi, X. Peng, M. Asaoka, J. Young, M. Opyrchal, L. Yan, S. Patnaik, E. Otsuji, et al. Tumor heterogeneity correlates with less immune response and worse survival in breast cancer patients. *Annals of surgical oncology*, 26(7):2191–2199, 2019.

[58] N. McGranahan and C. Swanton. Clonal heterogeneity and tumor evolution: past, present, and the future. *Cell*, 168(4):613–628, 2017.

[59] N. McGranahan, A. J. Furness, R. Rosenthal, S. Ramskov, R. Lyngaa, S. K. Saini, M. Jamal-Hanjani, G. A. Wilson, N. J. Birkbak, C. T. Hiley, et al. Clonal neoantigens elicit t cell immunoreactivity and sensitivity to immune checkpoint blockade. *Science*, 351(6280):1463–1469, 2016.

[60] J. L. Messerschmidt, G. C. Prendergast, and G. L. Messerschmidt. How cancers escape immune destruction and mechanisms of action for the new significantly active immune therapies: Helping nonimmunologists decipher recent advances. *The oncologist*, 21(2):233, 2016.

[61] N. Metropolis, A. W. Rosenbluth, M. N. Rosenbluth, A. H. Teller, and E. Teller. Equation of state calculations by fast computing machines. *The journal of chemical physics*, 21(6): 1087–1092, 1953.

[62] M. J. Miller, S. H. Wei, M. D. Cahalan, and I. Parker. Autonomous t cell trafficking examined in vivo with intravital two-photon microscopy. *Proceedings of the National Academy of Sciences*, 100(5):2604–2609, 2003.

[63] P. C. Nowell. The clonal evolution of tumor cell populations. *Science*, 194(4260):23–28, 1976.

[64] K. J. Painter and T. Hillen. Navigating the flow: individual and continuum models for homing in flowing environments. *Journal of The Royal Society Interface*, 12(112):20150647, 2015.

[65] J. Parkin and B. Cohen. An overview of the immune system. *The Lancet*, 357(9270):1777–1789, 2001.

[66] K. A. Rejniak and A. R. Anderson. Hybrid models of tumor growth. *Wiley Interdisciplinary Reviews: Systems Biology and Medicine*, 3(1):115–125, 2011.

[67] A. Reuben, R. Gittelman, J. Gao, J. Zhang, E. C. Yusko, C.-J. Wu, R. Emerson, J. Zhang, C. Tipton, J. Li, et al. Tcr repertoire intratumor heterogeneity in localized lung adenocarcinomas: an association with predicted neoantigen heterogeneity and postsurgical recurrence. *Cancer discovery*, 7(10):1088–1097, 2017.

[68] A. Ribas and J. D. Wolchok. Cancer immunotherapy using checkpoint blockade. *Science*, 359(6382):1350–1355, 2018.

[69] R. M. Samstein, C.-H. Lee, A. N. Shoushtari, M. D. Hellmann, R. Shen, Y. Y. Janjigian, D. A. Barron, A. Zehir, E. J. Jordan, A. Omuro, et al. Tumor mutational load predicts survival after immunotherapy across multiple cancer types. *Nature genetics*, 51(2):202–206, 2019.

[70] A. Snyder, V. Makarov, T. Merghoub, J. Yuan, J. M. Zaretsky, A. Desrichard, L. A. Walsh, M. A. Postow, P. Wong, T. S. Ho, et al. Genetic basis for clinical response to ctla-4 blockade in melanoma. *New England Journal of Medicine*, 371(23):2189–2199, 2014.

[71] R. Soiffer, F. S. Hodi, F. Haluska, K. Jung, S. Gillessen, S. Singer, K. Tanabe, R. Duda, S. Mentzer, M. Jaklitsch, et al. Vaccination with irradiated, autologous melanoma cells engineered to secrete granulocyte-macrophage colony-stimulating factor by adenoviral-mediated gene transfer augments antitumor immunity in patients with metastatic melanoma. *Journal of clinical oncology*, 21(17):3343–3350, 2003.

[72] R. Stace, T. Stiehl, M. Chaplain, A. Marciniak-Czochra, and T. Lorenzi. A phenotype-structured individual-based model for the evolution of cancer cell populations under chemotherapy. *Preprint*, 2019.

[73] M. H. Swat, G. L. Thomas, J. M. Belmonte, A. Shirinifard, D. Hmeljak, and J. A. Glazier. Multi-scale modeling of tissues using compucell3d. In *Methods in cell biology*, volume 110, pages 325–366. Elsevier, 2012.

[74] S. L. Topalian, C. G. Drake, and D. M. Pardoll. Immune checkpoint blockade: a common denominator approach to cancer therapy. *Cancer cell*, 27(4):450–461, 2015.

[75] O. Trédan, C. M. Galmarini, K. Patel, and I. F. Tannock. Drug resistance and the solid tumor microenvironment. *Journal of the National Cancer Institute*, 99(19):1441–1454, 2007.

[76] E. M. Van Allen, D. Miao, B. Schilling, S. A. Shukla, C. Blank, L. Zimmer, A. Sucker, U. Hillen, M. H. G. Foppen, S. M. Goldinger, et al. Genomic correlates of response to ctla-4 blockade in metastatic melanoma. *Science*, 350(6257):207–211, 2015.

[77] E. J. Wherry. T cell exhaustion. *Nature immunology*, 12(6):492–499, 2011.

[78] Y. Wolf, O. Bartok, S. Patkar, G. B. Eli, S. Cohen, K. Litchfield, R. Levy, A. Jiménez-Sánchez, S. Trabish, J. S. Lee, et al. Uvb-induced tumor heterogeneity diminishes immune response in melanoma. *Cell*, 179(1):219–235, 2019.

[79] J. S. Yi, M. A. Cox, and A. J. Zajac. T-cell exhaustion: characteristics, causes and conversion. *Immunology*, 129(4):474–481, 2010.

[80] E. I. Zuniga and J. A. Harker. T-cell exhaustion due to persistent antigen: Quantity not quality? *European journal of immunology*, 42(9):2285–2289, 2012.